Letter

Carrier-induced transition from antiferromagnetic insulator to ferromagnetic metal in the layered phosphide $EuZn_2P_2$

Xiyu Chen [1], Wuzhang Yang,[2,3] Jia-Yi Lu,[4] Zhiyu Zhou,[1] Zhi Ren,[2,3] Guang-Han Cao,[4,5] Shuai Dong [1], and Zhi-Cheng Wang [1,*]

[1]*Key Laboratory of Quantum Materials and Devices of Ministry of Education, School of Physics, Southeast University, Nanjing 211189, China*

[2]*School of Science, Westlake University, Hangzhou 310024, China*

[3]*Institute of Natural Sciences, Westlake Institute for Advanced Study, Hangzhou 310024, China*

[4]*School of Physics, Interdisciplinary Center for Quantum Information and State Key Laboratory of Silicon and Advanced Semiconductor Materials, Zhejiang University, Hangzhou 310058, China*

[5]*Collaborative Innovation Centre of Advanced Microstructures, Nanjing University, Nanjing 210093, China*

(Received 12 February 2024; revised 25 March 2024; accepted 8 May 2024; published 22 May 2024)

$EuZn_2P_2$ was reported to be an insulating antiferromagnet with T_N of 23.5 K. In this study single crystals of $EuZn_2P_2$ exhibiting metallic behavior and a ferromagnetic order of 72 K (T_C) are successfully synthesized via a salt flux method. The presence of hole carriers induced by the Eu vacancies in the lattice is found to be crucial for the drastic changes in magnetism and electrical transport. The carriers mediate the interlayer ferromagnetic interaction, and the coupling strength is directly related to T_C, as evidenced by the linear dependence of T_C and the fitted Curie-Weiss temperatures on the Eu-layer distances for ferromagnetic EuM_2X_2 (M = Zn, Cd; X = P, As). The ferromagnetic $EuZn_2P_2$ shows conspicuous negative magnetoresistance (MR) near T_C owing to strong magnetic scattering. The MR behavior is consistent with the Majumdar-Littlewood model, indicating that the MR can be enhanced by decreasing the carrier density. Our findings suggest that EuM_2X_2 has highly tunable magnetism and charge transport, making it a promising material family for potential applications in spintronics.

DOI: 10.1103/PhysRevB.109.L180410

Eu-based layered compounds of EuM_2X_2 (M = Zn, Cd; X = P, As, Sb) with a trigonal $CaAl_2Si_2$-type structure attract great research attention for the successive discoveries of exciting phenomena. $EuCd_2As_2$ was claimed to be a magnetic Weyl semimetal in the polarized state [1–6], and dramatic alterations in the magnetic ground state and charge transport were observed by applying pressure or changing the crystal growth condition [7–11]. $EuCd_2P_2$ shows a colossal magnetoresistance (CMR) effect due to the strong magnetic fluctuations well above the Néel temperature (T_N) at 11 K [12], and the onset of ferromagnetic (FM) order was discovered in the temperature range of the strongest CMR [13–15]. The insulator-to-metal transition as well as the topological phase transition was observed for pressurized $EuZn_2As_2$ [16]. Moreover, a CMR effect is also reported for $EuZn_2P_2$ with semiconducting behavior recently [17].

However, the physical properties reported with samples grown by different recipes are not consistent. For example, the perspective that $EuCd_2As_2$ is a topological semimetal was challenged by fresh experimental and theoretic evidence that indicates $EuCd_2As_2$ is in fact a magnetic semiconductor [18,19]. In addition, insulating behavior of $EuZn_2P_2$ was also reported in previous experiments [20,21]. The varied measurement results suggest the properties of materials in the EuM_2X_2 family are extremely sensitive to carrier concentration, which is usually induced unintentionally by vacancies in the sample.

In this study we report the successful synthesis of single crystals of $EuZn_2P_2$ (T_C = 72 K), $EuZn_2As_2$ (T_C = 42 K), and $EuCd_2P_2$ (T_C = 47 K) with a FM ground state. Comprehensive characterizations of magnetism and electrical transport for FM-$EuZn_2P_2$ are presented in the main text. We conclude that the heavy hole doping in FM-$EuZn_2P_2$ resulting from the Eu vacancies (∼5%) is responsible for the interlayer FM coupling, which leads to a transition from an antiferromagnetic (AFM) insulator to the FM metal. We find that these FM-EuM_2X_2, including FM-$EuCd_2As_2$ (T_C = 26 K) reported before [9], show a linear relationship between the Curie-Weiss temperatures θ_{CW} (as well as T_C) and the Eu-layer distances. This observation not only indicates the prominent role of interlayer Eu-Eu interaction in T_C, but also suggests the probability of T_C promotion by decreasing the layer distance. The switchable magnetic states and charge-transport behaviors make $EuZn_2P_2$ an excellent candidate for future spintronics.

Single crystals of FM-$EuZn_2P_2$ were grown via a molten salt flux, similar to the growth of FM-$EuCd_2As_2$ [9]. The details related to the sample growth can be found in the Supplemental Material (SM) [22]. Figure 1 displays the x-ray diffraction (XRD) pattern of FM-$EuZn_2P_2$ single crystal. Only sharp (00l) diffraction peaks were observed, indicating the high quality of the single crystals. Typically, the crystals grow as millimeter-sized hexagonal thin flakes, as shown in the left inset. The right inset illustrates the structure of $EuZn_2P_2$ that comprises alternating layers of triangular Eu^{2+} lattice connected by the layer of edge-sharing ZnP_4 tetrahedra. The crystallographic c axis, i.e., the distance of Eu

*wzc@seu.edu.cn

 ©2024 American Physical Society

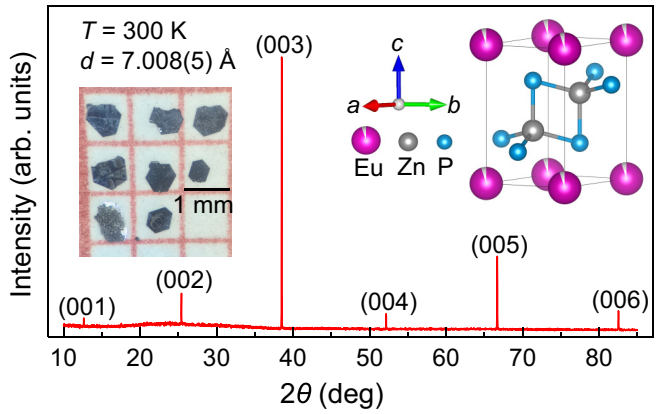

FIG. 1. XRD pattern ($\theta - 2\theta$ scan) of the FM-$EuZn_2P_2$ single crystal showing only (00l) reflections. Left inset shows the shape and size of typical FM-$EuZn_2P_2$ single crystals, and the right inset shows the crystal structure of $EuZn_2P_2$ with Eu vacancies.

layers, is calculated to be 7.008(5) Å with (00l) reflections. To further analyze the crystal structure of FM-$EuZn_2P_2$, the single-crystal XRD (SCXRD) data were collected at T = 150 K. The refined result (see Table I) confirms the $CaAl_2Si_2$-type structure of FM-$EuZn_2P_2$, and reveals 5% Eu vacancies in the lattice, consistent with a chemical composition resulting from energy-dispersive x-ray spectroscopy (EDX, Table S1 in SM) [22]. Compared to the structural parameters reported for AFM-$EuZn_2P_2$ at 213 K [20], FM-$EuZn_2P_2$ has a smaller unit cell due to the lower experimental temperature, but its c/a ratio is slightly larger (1.7156 vs 1.7141 for AFM-$EuZn_2P_2$), agreeing with the c-axis expansion caused by the hole doping. In a very recent study on AFM-$EuZn_2P_2$, the interlayer AFM coupling was explained as realized by the superexchange interaction through the Eu-P-P-Eu path [21]. Since the Eu-P and P-P bond lengths as well as the Eu-P-P bond angle are basically unchanged, and no vacancies are found for Zn_2P_2 layers of FM-$EuZn_2P_2$, it is plausible to assume that the interlayer AFM interaction is kept. Hence, the emerging ferromagnetism should be ascribed to the interlayer FM coupling mediated by the hole carriers. Although the substitution of Na^+/K^+ for Eu^{2+} will also result in hole doping, we conclude that the carriers are mainly induced by Eu vacancies, since Na/K is absent from EDX and the heterovalent substitution in EuM_2X_2 seems to be hard in a previous report [23]. In addition, the lattice strain caused by the minor contraction of unit cell (∼0.5%) is not likely to be the cause of the alterations of properties either, which is evidenced by a recent study about the pressure effect on insulating $EuCd_2As_2$ [24].

TABLE I. Crystallographic data and refinement result of FM-$EuZn_2P_2$ from the SCXRD at 150 K [25]. The occupancies of Zn and P were fixed to 1.0 to avoid unphysical values greater than 1.

Material	FM-$EuZn_2P_2$
Crystal system	Trigonal
Space group	$P\bar{3}m1$ (No. 164)
a (Å)	4.0765(2)
c (Å)	6.9936(4)
c/a	1.7156
V (Å^3)	100.648(11)
Z	1
Eu site occupancy	0.950(8)
Temperature (K)	150
Radiation	Mo $K\alpha$
Reflections collected	1424
Independent reflections	104
R_{int}	0.0819
Goodness-of-fit	1.345
R_1[a]	0.0339
wR_2[b]	0.0984
Fractional coordinates	
Eu	(0,0,0)
Zn	(1/3,2/3,0.6305(4))
P	(1/3,2/3,0.2691(7))

[a] $R_1 = \Sigma||F_o| - |F_c||/\Sigma|F_o|$.
[b] $wR_2 = [\Sigma w(F_o^2 - F_c^2)^2/\Sigma w(F_o^2)^2]^{1/2}$.

The magnetism of FM-$EuZn_2P_2$ is summarized in Fig. 2. A clear hysteresis loop can be found for the $M(H)$ curve with the in-plane field ($H \parallel ab$) at 1.8 K, shown in panel (a). And the hysteresis loop with the out-of-plane field is indistinctive ($H \parallel c$) compared to the in-plane curve, suggesting that the spins should be aligned in the ab plane, as illustrated by the inset. Recent studies have demonstrated that the magnetic ordering of AFM-$EuZn_2P_2$ is A type, i.e., in-plane FM coupling and out-of-plane AFM coupling, whose $M(H)$ curves do not exhibit any hysteresis [17,20,21]. The significant difference in $M(H)$ curves between AFM- and FM-$EuZn_2P_2$ indicates that the intrinsic FM-$EuZn_2P_2$ is successfully prepared by changing the growth condition.

Figure 2(b) displays the comparison of $M(H)$ curves between FM- and AFM-$EuZn_2P_2$. For FM-$EuZn_2P_2$, the $M(H)$ curves exhibit strong magnetocrystalline anisotropy. The saturation field (H_{sat}) for the in-plane magnetization is only about 0.1 T, while the out-of-plane magnetization increases rapidly below 0.1 T and finally saturates at the field over 2.5 T. The similar metamagnetic transition around 0.1 T with the c-axis field was also reported for FM-$EuCd_2As_2$, which was attributed to the increasing canting of spins in the external field [10]. The large magnetocrystalline anisotropy (over 25 times on the basis of H_{sat}) suggests that the Eu layer (the ab plane) is the magnetic easy plane. We notice that the values of H_{sat} ($H \parallel c$) for FM- and AFM-$EuZn_2P_2$ are comparable, while H_{sat} of FM-$EuCd_2As_2$ for $H \parallel ab$ is noticeably reduced. The conspicuous change in H_{sat} manifests that the FM coupling between the Eu layers is much enhanced by the induced carries. In addition, the saturated magnetizations (M_{sat}) of FM-$EuZn_2P_2$ reach about 7 μ_B for both directions at 1.8 K, consistent with the Eu^{2+} oxidation state.

Figures 2(c) and 2(d) show the curves of temperature-dependent magnetic susceptibility of FM-$EuZn_2P_2$ under the in-plane and out-of-plane magnetic fields, respectively. Both $\chi_{ab}(T)$ and $\chi_c(T)$ increase dramatically below 80 K, and evident bifurcations of zero-field-cooling (ZFC) and field-cooling (FC) data are observed with small fields, which is the typical feature for ferromagnets and is consistent with the hysteresis loops in Fig. 2(a). The splittings are rapidly suppressed with the increasing field. The Curie temperature (T_C) of FM-$EuZn_2P_2$ is determined by the susceptibility

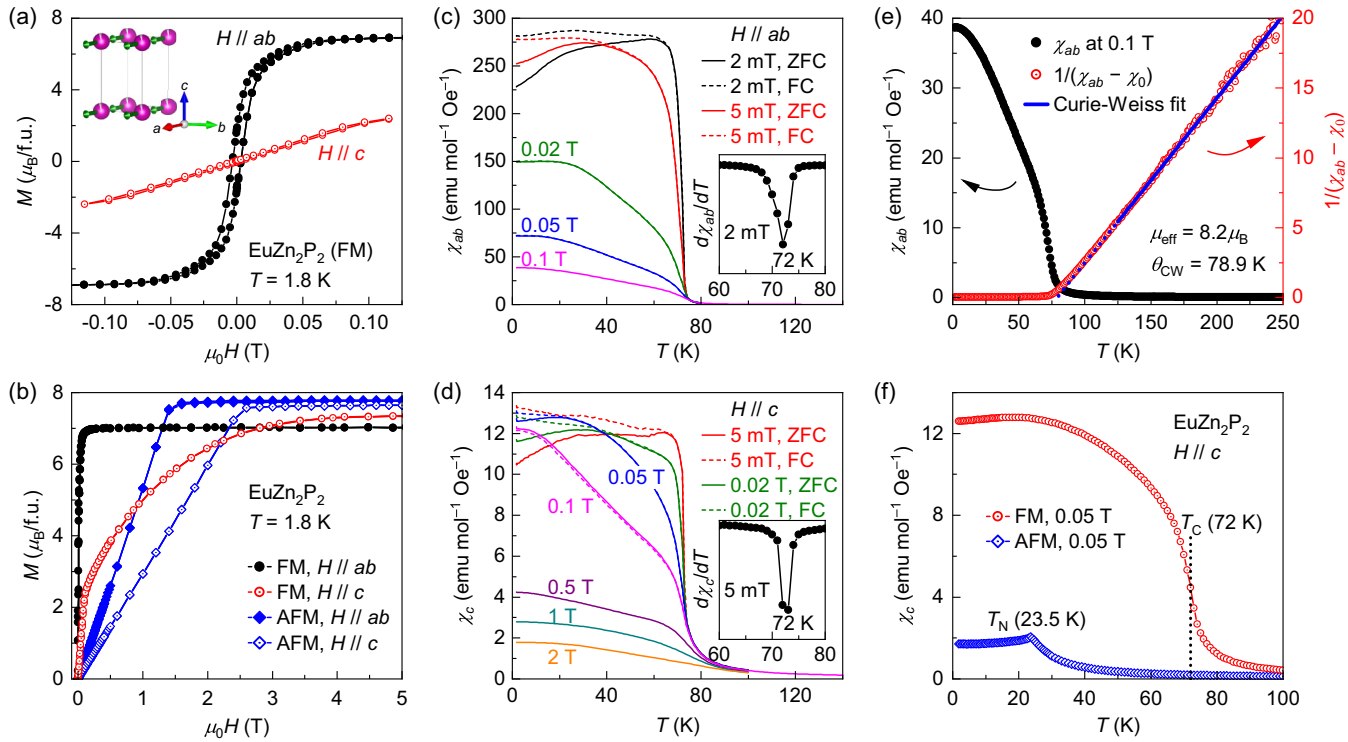

FIG. 2. (a) Magnetic hysteresis loops of FM-$EuZn_2P_2$ at 1.8 K for fields in the *ab* plane (black) and along the *c* axis (red). Inset shows the spin configuration of FM-$EuZn_2P_2$. (b) Magnetization as a function of field for FM- (black and red circles) and AFM- (blue diamonds) $EuZn_2P_2$ at $T = 1.8$ K. (c), (d) Temperature dependences of magnetic susceptibility for field parallel to the *ab* plane (c) and the *c* axis (d). Their insets present the derivative of the magnetic susceptibility ($d\chi/dT$) to show the transition temperatures. (e) Curie-Weiss analysis from 125 to 300 K with $\chi_{ab}(T)$ data at 0.1 T. Only data below 250 K are shown. (f) The magnetic transitions for FM- (red) and AFM-$EuZn_2P_2$ (blue) at 0.05 T.

derivatives ($d\chi/dT$), shown in the insets of Figs. 2(c) and 2(d). T_C is identified to be 72 K by both $d\chi_{ab}/dT$ and $d\chi_c/dT$. Moreover, we notice that χ_{ab} is about an order of magnitude larger than χ_c for the small fields, which confirms the strong magnetocrystalline anisotropy of FM-$EuZn_2P_2$ in Figs. 2(a) and 2(b).

The Curie-Weiss analysis of $\chi_{ab}(T)$ is presented in Fig. 2(e). The data above 125 K is fitted with $\chi_{ab} = \chi_0 + C/(T - \theta_{CW})$, which yields $C = 8.47$ emu K mol^{-1} Oe^{-1} (effective moment $\mu_{eff} = 8.2\,\mu_B$/f.u.), $\theta_{CW} = 78.9$ K, and $\chi_0 = 1.39 \times 10^{-4}$ emu mol^{-1} Oe^{-1}. The value of μ_{eff} is coincident with the theoretical value of $7.94\,\mu_B$ for Eu^{2+}. The Curie-Weiss temperature θ_{CW} is close to the experimentally determined T_C, indicating that $EuZn_2P_2$ is manipulated to be an intrinsic ferromagnet rather than a canted antiferromagnet. $\chi_c(T)$ of AFM- and FM-$EuZn_2P_2$ are compared in Fig. 2(f). AFM-$EuZn_2P_2$ exhibits a conspicuous peak at 23.5 K, agreeing well with the reported Néel temperature (T_N) [17,20,21]. The distinct behaviors of $\chi_c(T)$ confirm the alteration of ground-state and the dominant FM interaction in FM-$EuZn_2P_2$. T_C of FM-$EuZn_2P_2$ is significantly higher than those of the sister materials with a FM state (47 K for $EuCd_2P_2$, 26 K for $EuCd_2As_2$, 42 K for $EuZn_2As_2$, see SM) [22], which is attributed to its smaller distance of Eu layers and is discussed later.

FM-$EuZn_2P_2$ exhibits a metallic behavior, as shown in Fig. 3(a). In the paramagnetic (PM) region (above 120 K), the zero-field in-plane resistivity (ρ_{ab}) decreases as the temperature goes down, and then shows a mild rise in the region of magnetic fluctuation ($T_C \lesssim T \lesssim 1.5T_C$) due to the enhanced scattering. Finally, ρ_{ab} decreases monotonically below the FM ordering at 72 K. The residual resistivity ratio (RRR, a ratio of R_{300K} and R_{0K}) is 6 and remains almost unchanged in the field. Considering 5% Eu^{2+} vacancies in the lattice, the hole concentration in FM-$EuZn_2P_2$ is estimated to be 10^{21} cm^{-3} based on the single-band model, which results in the Mott-Ioffe-Regel (MIR) limit of 0.7 mΩ cm [26]. Since the residual resistivity at 2 K (∼ 0.2 mΩ cm) is below the MIR limit, FM-$EuZn_2P_2$ is a good metal with a relatively long mean free path. We found that the behavior of zero field $\rho_{ab}(T)$ below 50 K could be well described with a simple quadratic function $\rho(T) = \rho_0 + AT^2$, where the T^2 dependence is contributed by the electron-electron or electron-magnon scattering. The resultant fitting parameters are $\rho_0 = 0.193$ mΩ cm, $A = 9.60 \times 10^{-5}$ mΩ cm K^{-2}. The typical Fermi liquid behavior indicates the negligible electron-phonon scattering at low temperatures and the weak electron correlation of FM-$EuZn_2P_2$.

The resistivity peak at T_C is suppressed by applying the external magnetic fields. The curves of ρ_{ab} as a function of field are plotted in Fig. 3(b). The maximum negative magnetoresistance (MR) is achieved at T_C, which is over −50% at 8 T with the definition MR = $100\% \times [\rho(H) - \rho(0)]/\rho(0)$. For the temperatures well below T_C, the negative MR is weak and a small enhancement in $\rho_{ab}(H)$ is observed when the field is low, which is also seen for FM-$EuCd_2As_2$ and should be

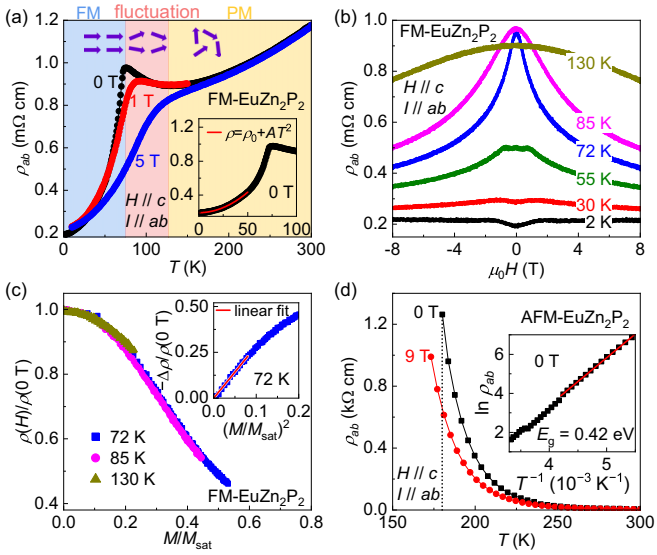

FIG. 3. (a) In-plane resistivity of FM-$EuZn_2P_2$ as a function temperature under several fields. Inset shows a fit (red curve) with the parabolic function $\rho(T) = \rho_0 + AT^2$ to the zero-field resistivity below 50 K. (b) Field-dependent resistivity of FM-$EuZn_2P_2$ at various temperatures from 2 to 130 K. (c) Normalized resistivity $\rho(H)/\rho(0\ \mathrm{T})$ at 72 K (blue squares), 85 K (magenta circles), and 130 K (dark yellow triangles) plotted against normalized field-induced magnetization M/M_{sat}, where M_{sat} is the saturated magnetization, i.e., 7 μ_B. Inset plots $-$MR as a function of $(M/M_{\mathrm{sat}})^2$ and a linear fit (red line) for $(M/M_{\mathrm{sat}})^2 \leqslant 0.08$. (d) In-plane resistivity of AFM-$EuZn_2P_2$ at 0 and 9 T. Inset displays the Arrhenius plot ($\ln \rho_{ab}$ vs T^{-1}) of zero-field data, as well as a linear fit (red line).

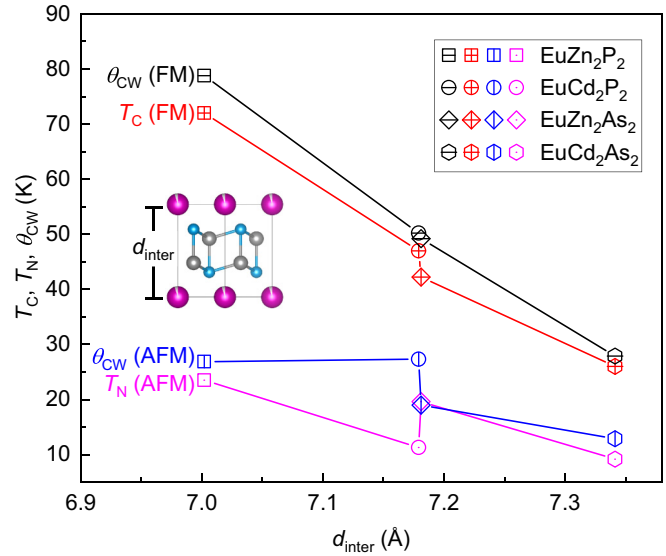

FIG. 4. The characteristic temperatures (T_C, T_N, θ_{CW}) of EuM_2X_2 (M = Zn, Cd; X = P, As) as a function of the Eu-layer distance, i.e., the c axis. The squares, circles, diamonds, and hexagons represent the data of $EuZn_2P_2$, $EuCd_2P_2$, $EuZn_2As_2$, and $EuCd_2As_2$, respectively. The error bars are not shown because the uncertainties of data points are smaller than the size of symbols.

related to the increased canting of spins towards the c axis in the field [10]. The normalized resistivity $\rho(H)/\rho(0\ \mathrm{T})$ at 72 K (T_C), 85 K ($1.2T_C$), and 130 K ($1.8T_C$) against normalized magnetization (M/M_{sat}) is plotted in Fig. 3(c). The resistivity at three different temperatures changes with magnetization by following a similar trace. The good correlation implies that the MR of FM-$EuZn_2P_2$ is closely related to the magnetization, which means that magnetic scattering plays a major role in the MR of FM-$EuZn_2P_2$. In the inset of Fig. 3(c), we plot $-$MR at 72 K, i.e., $-\Delta\rho/\rho(0\ \mathrm{T})$, as a function of $(M/M_{\mathrm{sat}})^2$. It is seen that the magnitude of $-$MR obeys the scaling function

$$-\Delta\rho/\rho(0\ \mathrm{T}) = C_{\mathrm{MR}}(M/M_{\mathrm{sat}})^2 \qquad (1)$$

in the relatively low-M region, say $M/M_{\mathrm{sat}} \leqslant 0.3$. The scaling factor C_{MR} is 2.85, resulting from the linear fit with the data in low-M region. Since the metallic transport of FM-$EuZn_2P_2$, the Majumdar-Littlewood model is applicable to elucidate the dependence of MR on charge-carrier density [27]. According to the model, C_{MR} could be estimated with the relation $C_{\mathrm{MR}} \approx x^{-2/3}$, where x is the number of charge carriers per magnetic unit cell. In the case of FM-$EuZn_2P_2$, $x \approx 0.1$ due to 5% Eu^{2+} vacancies. Then we have $C_{\mathrm{MR}} = 4.6$, comparable to the fitting value. Hence, the enhanced MR effect of FM-$EuZn_2P_2$ is expected by simply declining the carrier concentration, which could be realized through chemical doping or electrostatic gating.

We also measured the in-plane resistivity of AFM-$EuZn_2P_2$ for comparison, which is three orders of magnitude higher than that of FM-$EuZn_2P_2$ at 300 K, as shown in Fig. 3(d). AFM-$EuZn_2P_2$ is insulating without the magnetic field. By applying a field of 9 T, ρ_{ab} declines by half at 180 K, yet the insulating behavior is retained. The band gap is estimated to be 0.42 eV with the Arrhenius model $\rho \propto e^{E_g/2k_BT}$, consistent with earlier studies [20,21]. The distinct charge-transport behaviors of FM- and AFM-$EuZn_2P_2$ demonstrate that this system is successfully tuned from an AFM insulator into a FM metal by inducing the carriers.

To get a deeper understanding of the carrier-induced ferromagnetism in EuM_2X_2 (M = Zn, Cd; X = P, As), we synthesized FM-$EuZn_2As_2$ ($T_C = 42$ K) and FM-$EuCd_2P_2$ ($T_C = 47$ K) via the salt flux method as well. The characterizations of magnetism are presented in Figs. S3 and S4 in the SM [22]. The characteristic temperatures (T_C, T_N, θ_{CW}) of both FM- and AFM-EuM_2X_2 are plotted as a function of the Eu-layer distance (d_{inter}) in Fig. 4. Note that since the structural difference between EuM_2X_2 with the FM and AFM states is pretty small, we use the c-axis value reported for AFM-EuM_2X_2 at room temperature as d_{inter} for both materials [9,12,20,28]. T_N and θ_{CW} of AFM-EuM_2X_2 do not show a monotonic dependence on d_{inter}, while T_C and θ_{CW} of FM-EuM_2X_2 increase almost linearly with decreasing d_{inter}. These linear relationships convincingly demonstrate that the FM ordering temperatures of FM-EuM_2X_2 mainly depend on the interlayer Eu-Eu coupling. Thus T_C could be further enhanced by applying pressure or doping smaller divalent ions such as Ca^{2+} to decrease the layer distance. Actually, T_C over 100 K was reported in pressurized $EuZn_2As_2$ [16]. We notice that all values of T_C are slightly smaller than the corresponding θ_{CW}, which is ascribed to the influence of existing interlayer AFM interaction through the Eu-X-X-Eu superexchange path, as mentioned earlier [21]. Therefore, it

is natural to see a larger discrepancy between T_C and θ_{CW} for FM-$EuZn_2P_2$ and FM-$EuZn_2As_2$ due to their shorter Eu-X-X-Eu path.

Our results manifest that the interlayer FM coupling is essential to the FM ordering temperature, and the FM interaction results from the indirect exchange mediated by carriers. The role of carrier densities has not been discussed yet. It seems that the influence of carrier concentration on T_C is not primary in the case of EuM_2X_2. For example, T_C and θ_{CW} of FM-$EuCd_2As_2$ vary only several kelvins when the chemical doping level changes by an order of magnitude [23]. Since the carrier concentrations of FM-EuM_2X_2 are lower than the validity condition of the Ruderman-Kittel-Kasuya-Yosida (RKKY) theory ($>10^{21}$ cm^{-3}), the dependence of interlayer FM interaction on the carrier density cannot be understood within this framework [29]. Nevertheless, the correlation between T_C and carrier density is not ruled out. Further theoretic and experimental efforts will be devoted to investigating the effect of carrier density on T_C.

In summary, FM-$EuZn_2P_2$ was successfully grown via the salt flux method, which has similar structural parameters to AFM-$EuZn_2P_2$ except for 5% Eu vacancies. The magnetization and resistivity measurements show that the defective $EuZn_2P_2$ is a FM metal of $T_C = 72$ K rather than an AFM insulator of $T_N = 23.5$ K, as in the vacancy-free version. The analysis of field-dependent resistivity indicates that the magnetic scattering makes the main contribution to the resistivity near T_C. On basis of the Majumdar-Littlewood model, a greater MR effect is probably achieved by reducing the carrier density. The transition temperatures and Curie-Weiss temperatures of AFM- and FM-EuM_2X_2 (M = Zn, Cd; X = P, As) are examined, which reveals linear dependences of θ_{CW} and T_C on the Eu-layer distance, indicating the critical role of interlayer FM coupling on the FM ordering. Our results suggest that FM coupling could be induced with low carrier densities in Eu-based $CaAl_2Si_2$-type materials, which may also be applicable to other AFM Eu-based Zintl compounds such as $EuIn_2As_2$ and $EuMn_2P_2$, for their narrow energy gaps and similar layered structures. Moreover, it is of great interest to explore other exotic phenomena such as the topological phase transition by tuning the carrier concentration of EuM_2X_2 in controlled manners like chemical doping and the gating technique, which is not only important for fundamental research, but also significant for potential applications in spintronics.

Acknowledgments. This work was supported by the National Natural Science Foundation of China (Grant No. 12204094), the Natural Science Foundation of Jiangsu Province (Grant No. BK20220796), the Start-up Research Fund of Southeast University (Grant No. RF1028623289), the Interdisciplinary program of Wuhan National High Magnetic Field Center (WHMFC) at Huazhong University of Science and Technology (Grant No. WHMFC202205), and the open research fund of Key Laboratory of Quantum Materials and Devices (Southeast University), Ministry of Education.

[1] G. Hua, S. Nie, Z. Song, R. Yu, G. Xu, and K. Yao, Dirac semimetal in type-IV magnetic space groups, Phys. Rev. B **98**, 201116(R) (2018).

[2] J.-R. Soh, F. de Juan, M. G. Vergniory, N. B. M. Schröter, M. C. Rahn, D. Y. Yan, J. Jiang, M. Bristow, P. Reiss, J. N. Blandy, Y. F. Guo, Y. G. Shi, T. K. Kim, A. McCollam, S. H. Simon, Y. Chen, A. I. Coldea, and A. T. Boothroyd, Ideal Weyl semimetal induced by magnetic exchange, Phys. Rev. B **100**, 201102(R) (2019).

[3] L.-L. Wang, N. H. Jo, B. Kuthanazhi, Y. Wu, R. J. McQueeney, A. Kaminski, and P. C. Canfield, Single pair of Weyl fermions in the half-metallic semimetal $EuCd_2As_2$, Phys. Rev. B **99**, 245147 (2019).

[4] M. C. Rahn, J.-R. Soh, S. Francoual, L. S. I. Veiga, J. Strempfer, J. Mardegan, D. Y. Yan, Y. F. Guo, Y. G. Shi, and A. T. Boothroyd, Coupling of magnetic order and charge transport in the candidate Dirac semimetal $EuCd_2As_2$, Phys. Rev. B **97**, 214422 (2018).

[5] J.-Z. Ma, S. M. Nie, C. J. Yi, J. Jandke, T. Shang, M. Y. Yao, M. Naamneh, L. Q. Yan, Y. Sun, A. Chikina, V. N. Strocov, M. Medarde, M. Song, Y.-M. Xiong, G. Xu, W. Wulfhekel, J. Mesot, M. Reticcioli, C. Franchini, C. Mudry *et al.*, Spin fluctuation induced Weyl semimetal state in the paramagnetic phase of $EuCd_2As_2$, Sci. Adv. **5**, eaaw4718 (2019).

[6] Y. Xu, L. Das, J. Z. Ma, C. J. Yi, S. M. Nie, Y. G. Shi, A. Tiwari, S. S. Tsirkin, T. Neupert, M. Medarde, M. Shi, J. Chang, and T. Shang, Unconventional transverse transport above and below the magnetic transition temperature in Weyl semimetal $EuCd_2As_2$, Phys. Rev. Lett. **126**, 076602 (2021).

[7] E. Gati, S. L. Bud'ko, L.-L. Wang, A. Valadkhani, R. Gupta, B. Kuthanazhi, L. Xiang, J. M. Wilde, A. Sapkota, Z. Guguchia, R. Khasanov, R. Valentí, and P. C. Canfield, Pressure-induced ferromagnetism in the topological semimetal $EuCd_2As_2$, Phys. Rev. B **104**, 155124 (2021).

[8] F. Du, L. Yang, Z. Nie, N. Wu, Y. Li, S. Luo, Y. Chen, D. Su, M. Smidman, Y. Shi, C. Cao, F. Steglich, Y. Song, and H. Yuan, Consecutive topological phase transitions and colossal magnetoresistance in a magnetic topological semimetal, npj Quantum Mater. **7**, 65 (2022).

[9] N. H. Jo, B. Kuthanazhi, Y. Wu, E. Timmons, T.-H. Kim, L. Zhou, L.-L. Wang, B. G. Ueland, A. Palasyuk, D. H. Ryan, R. J. McQueeney, K. Lee, B. Schrunk, A. A. Burkov, R. Prozorov, S. L. Bud'ko, A. Kaminski, and P. C. Canfield, Manipulating magnetism in the topological semimetal $EuCd_2As_2$, Phys. Rev. B **101**, 140402(R) (2020).

[10] S. Roychowdhury, M. Yao, K. Samanta, S. Bae, D. Chen, S. Ju, A. Raghavan, N. Kumar, P. Constantinou, S. N. Guin, N. C. Plumb, M. Romanelli, H. Borrmann, M. G. Vergniory, V. N. Strocov, V. Madhavan, C. Shekhar, and C. Felser, Anomalous Hall conductivity and Nernst effect of the ideal Weyl semimetallic ferromagnet $EuCd_2As_2$, Adv. Sci. **10**, 2207121 (2023).

[11] K. M. Taddei, L. Yin, L. D. Sanjeewa, Y. Li, J. Xing, C. dela Cruz, D. Phelan, A. S. Sefat, and D. S. Parker, Single pair of

Weyl nodes in the spin-canted structure of $EuCd_2As_2$, Phys. Rev. B **105**, L140401 (2022).

[12] Z.-C. Wang, J. D. Rogers, X. Yao, R. Nichols, K. Atay, B. Xu, J. Franklin, I. Sochnikov, P. J. Ryan, D. Haskel, and F. Tafti, Colossal magnetoresistance without mixed valence in a layered phosphide crystal, Adv. Mater. **33**, 2005755 (2021).

[13] V. Sunko, Y. Sun, M. Vranas, C. C. Homes, C. Lee, E. Donoway, Z.-C. Wang, S. Balguri, M. B. Mahendru, A. Ruiz, B. Gunn, R. Basak, S. Blanco-Canosa, E. Schierle, E. Weschke, F. Tafti, A. Frano, and J. Orenstein, Spin-carrier coupling induced ferromagnetism and giant resistivity peak in $EuCd_2P_2$, Phys. Rev. B **107**, 144404 (2023).

[14] C. C. Homes, Z.-C. Wang, K. Fruhling, and F. Tafti, Optical properties and carrier localization in the layered phosphide $EuCd_2P_2$, Phys. Rev. B **107**, 045106 (2023).

[15] H. Zhang, F. Du, X. Zheng, S. Luo, Y. Wu, H. Zheng, S. Cui, Z. Sun, Z. Liu, D. Shen, M. Smidman, Y. Song, M. Shi, Z. Zhong, C. Cao, H. Yuan, and Y. Liu, Electronic band reconstruction across the insulator-metal transition in colossally magnetoresistive $EuCd_2P_2$, Phys. Rev. B **108**, L241115 (2023).

[16] S. Luo, Y. Xu, F. Du, L. Yang, Y. Chen, C. Cao, Y. Song, and H. Yuan, Colossal magnetoresistance and topological phase transition in $EuZn_2As_2$, Phys. Rev. B **108**, 205140 (2023).

[17] S. Krebber, M. Kopp, C. Garg, K. Kummer, J. Sichelschmidt, S. Schulz, G. Poelchen, M. Mende, A. V. Virovets, K. Warawa, M. D. Thomson, A. V. Tarasov, D. Y. Usachov, D. V. Vyalikh, H. G. Roskos, J. Müller, C. Krellner, and K. Kliemt, Colossal magnetoresistance in $EuZn_2P_2$ and its electronic and magnetic structure, Phys. Rev. B **108**, 045116 (2023).

[18] D. Santos-Cottin, I. Mohelský, J. Wyzula, F. Le Mardelé, I. Kapon, S. Nasrallah, N. Barišić, I. Živković, J. R. Soh, F. Guo, K. Rigaux, M. Puppin, J. H. Dil, B. Gudac, Z. Rukelj, M. Novak, A. B. Kuzmenko, C. C. Homes, T. Dietl, M. Orlita *et al.*, $EuCd_2As_2$: A Magnetic Semiconductor, Phys. Rev. Lett. **131**, 186704 (2023).

[19] Y. Shi, Z. Liu, L. A. Burnett, S. Lee, C. Hu, Q. Jiang, J. Cai, X. Xu, C.-C. Chen, and J.-H. Chu, Absence of Weyl nodes in $EuCd_2As_2$ revealed by the carrier density dependence of the anomalous Hall effect, Phys. Rev. B **109**, 125202 (2024).

[20] T. Berry, V. J. Stewart, B. W. Y. Redemann, C. Lygouras, N. Varnava, D. Vanderbilt, and T. M. McQueen, A-type antiferromagnetic order in the Zintl-phase insulator $EuZn_2P_2$, Phys. Rev. B **106**, 054420 (2022).

[21] K. Singh, S. Dan, A. Ptok, T. A. Zaleski, O. Pavlosiuk, P. Wiśniewski, and D. Kaczorowski, Superexchange interaction in insulating $EuZn_2P_2$, Phys. Rev. B **108**, 054402 (2023).

[22] See Supplemental Material at http://link.aps.org/supplemental/10.1103/PhysRevB.109.L180410 for experimental details; chemical composition analysis of FM-$EuZn_2P_2$, AFM-$EuZn_2P_2$, and FM-$EuZn_2As_2$; structural analysis of AFM-$EuZn_2P_2$;and supporting data for magnetism of $EuZn_2P_2$, FM-$EuZn_2As_2$, and FM-$EuCd_2P_2$.

[23] B. Kuthanazhi, K. R. Joshi, S. Ghimire, E. Timmons, L.-L. Wang, E. Gati, L. Xiang, R. Prozorov, S. L. Bud'ko, and P. C. Canfield, Magnetism and T-x phase diagrams of Na- and Ag-substituted $EuCd_2As_2$, Phys. Rev. Mater. **7**, 034402 (2023).

[24] X. Chen, S. Wang, J. Wang, C. An, Y. Zhou, Z. Chen, X. Zhu, Y. Zhou, Z. Yang, and M. Tian, Temperature-pressure phase diagram of the intrinsically insulating topological antiferromagnet $EuCd_2As_2$, Phys. Rev. B **107**, L241106 (2023).

[25] CCDC 2330806 contains the supplementary crystallographic data for FM-$EuZn_2P_2$.

[26] M. Gurvitch, Ioffe-Regel criterion and resistivity of metals, Phys. Rev. B **24**, 7404 (1981).

[27] P. Majumdar and P. B. Littlewood, Dependence of magnetoresistivity on charge-carrier density in metallic ferromagnets and doped magnetic semiconductors, Nature (London) **395**, 479 (1998).

[28] Z.-C. Wang, E. Been, J. Gaudet, G. M. A. Alqasseri, K. Fruhling, X. Yao, U. Stuhr, Q. Zhu, Z. Ren, Y. Cui, C. Jia, B. Moritz, S. Chowdhury, T. Devereaux, and F. Tafti, Anisotropy of the magnetic and transport properties of $EuZn_2As_2$, Phys. Rev. B **105**, 165122 (2022).

[29] É. Nagaev, Indirect exchange in ferromagnets with low carrier densities, Zh. Eksp. Teor. Fiz. **90**, 652 (1986).